THE ASTROPHYSICAL JOURNAL, 398:495–500, 1992 October 20


# THE NEAR-ULTRAVIOLET SPECTRUM OF MARKARIAN 205[1]

JOHN N. BAHCALL, BUELL T. JANNUZI, AND DONALD P. SCHNEIDER
Institute for Advanced Study, School of Natural Sciences, Princeton, NJ 08540
GEORGE F. HARTIG
Space Telescope Science Institute, 3700 San Martin Drive, Baltimore, MD 21218
AND
EDWARD B. JENKINS
Princeton University Observatory, Princeton, NJ 08544
*Received 1992 February 24; accepted 1992 April 23*

## ABSTRACT

We report measurements of the absorption and of the emission lines between 1600 and 3200 Å in the spectrum of the nearby AGN Markarian 205 ($z = 0.071$), which lies at a projected distance of 3 kpc ($H_0 = 100$ km s$^{-1}$) from the nucleus of the nearby barred spiral galaxy, NGC 4319 ($z = 0.0047$). The results were obtained using high-resolution ($R = 1300$) observations with the Faint Object Spectrograph of the *Hubble Space Telescope*. A total of 15 absorption lines, 13 of which are produced by Galactic gas, and four AGN emission lines are detected.

Two of the absorption lines, the Mg II resonant doublet, are produced by gas in the intervening galaxy NGC 4319. This is the first detection of absorption due to intervening gas in this famous quasar-galaxy pair.

*Subject headings:* galaxies: active — galaxies: individual (Markarian 205, NGC 4319) — galaxies: Seyfert

## 1. INTRODUCTION

Quasars that lie behind nearby galaxies can be used to explore the gaseous content of Galactic disks and halos in much the same way that metal line absorption systems seen in large redshift quasars are believed to reveal properties of very distant (usually undetected) galaxies. We concentrate in this paper on the gas in the interstellar medium and in the halo of NGC 4319, a bright spiral galaxy whose nucleus lies at a projected distance of 3 kpc ($H_0 = 100$ km s$^{-1}$) from the AGN Mrk 205. The spectrum of Mrk 205 contains information about both the disk gas and the halo gas of NGC 4319, since (on the cosmological hypothesis, see below) the light from the AGN Mrk 205 passes through the face-on galaxy on the way to the observer.

Mrk 205 is a relatively nearby ($z_{em} = 0.071$) and bright ($V = 15.2$ mag) Seyfert I galaxy (Markarian 1969; Véron-Cetty & Véron 1991) or low-luminosity quasar (Shuder 1984). Weedman (1970) first called special attention to this AGN because the nucleus of the galaxy lies within 0.7 of a bright barred spiral galaxy, NGC 4319. In fact, Mrk 205 is projected on the sky at a position within the spiral arms of the nearby galaxy NGC 4319, which has a heliocentric velocity of only about 1405 km s$^{-1}$ or $z = 0.00468$ (Bowen et al. 1991; Sulentic & Arp 1987a). The factor of more than 10 difference between the redshifts of the galaxy and the AGN has provoked much discussion concerning a possible physical association between the AGN and the galaxy, the suggested connection being interpreted as evidence for a noncosmological redshift (Weedman 1970; Arp 1971; Arp 1973; Sulentic & Arp 1987a, b; Burbidge 1988 and references therein; counter arguments have been presented in Bahcall 1973; Bowen et al. 1991 and references therein). Some particularly beautiful pictures of this galaxy-AGN pair have been published by Sulentic & Arp (1987a).

Bowen et al. (1991), using ground-based observations, derived a surprisingly small upper limit, 0.038 Å (2 $\sigma$), on the Ca II K absorption-line equivalent width produced by the gaseous material of NGC 4319. This upper limit is much smaller than the estimated modal value of 0.220 Å (Bowen et al. 1991) that would result from a face-on transversal of the Galaxy near the solar position and is also much less than the Ca II K equivalent widths produced by the interstellar media and halos of external galaxies as seen in the spectra of extragalactic supernovae. Using *IUE* spectra, Kinney et al. (1991) and Bowen et al. (1991) derived a 2 $\sigma$ limit of 0.7 Å for the Mg II resonance lines. This nondetection is also significantly smaller than the typical strength of Mg II absorption in the Galactic disk and halo (see Savage & de Boer 1981; Savage 1988; Blades et al. 1988). The failure to detect absorption from Ca II or Mg II in the interstellar gas or in the halo gas of NGC 4319 prompted Bowen et al. (1991) to consider a variety of explanations, including the possibility that Mrk 205 is not at the distance indicated by its redshift but instead lies in front of NGC 4319.

In what follows, we assume the conventional cosmological interpretation of the redshift of Mrk 205, according to which the AGN lies behind the barred spiral NGC 4319. The chance positioning of Mrk 205 behind NGC 4319 offers a rare opportunity to probe the metallic content of the interstellar and halo gas of a nearby galaxy.

This paper describes our high-resolution ultraviolet observations of Mrk 205 made on 11 July 1991 with the Faint Object Spectrograph (FOS; see Ford 1985) of the *Hubble Space Telescope* (*HST*). The paper is organized as follows: observations (§ 2), continuum and emission lines (§ 3), measurement of the absorption lines (§ 4), Galactic absorption lines (§ 5), and absorption features caused by gas in NGC 4319 (§ 6). We summarize and discuss our main results in § 7.

[1] Based on observations with the NASA/ESA *Hubble Space Telescope*, obtained at the Space Telescope Science Institute, which is operated by the Association of Universities for Research in Astronomy, Inc., under NASA contract NAS5-26555.

In this paper we only summarize the procedures we have used in reducing the data, in measuring the emission and absorption lines, and in identifying the absorption lines; a more detailed discussion is given in Bahcall et al. (1992).

## 2. OBSERVATIONS

We observed Mrk 205 with two high-resolution ($R = 1300$) gratings, G190H and G270H, using the red detector of the FOS; the gratings are centered, respectively, on 1900 and 2700 Å. The spectra cover, with good signal-to-noise ratio (S/N), the region between 1650 and 3270 Å. The data were obtained with the 0.″25 × 2.″0 slit.

The dispersions in the G190H and G270H data are, respectively, 0.36 and 0.52 Å pixel$^{-1}$, with approximate spectral resolutions (FWHMs) of 1.5 and 2.0 Å for the two gratings. The observations were read out every 40 s in order to avoid a reduction in the spectral resolution caused by insufficient magnetic shielding in the FOS. Corrections for magnetic-field induced wavelength shifts were made with the software developed by the FOS instrument definition team (see Beaver et al. 1991). Wavelength offsets for the different gratings were computed so that the strong Galactic absorption lines are at rest.

Residual errors in the flat-fielding dominate the statistical noise in some portions of the spectrum and create spurious weak features. Since the strengths of features in the flat fields seem to be increasing with time, it is important to use a flat-field observation that was taken as close as possible to the epoch of the science observation. Corrections made in this paper for variations in the sensitivity of the photocathodes and of the diodes were based upon observations of the white dwarf KPD 0005+5106 (see Bohlin et al. 1990), which were taken within 2 weeks of our observations of Mrk 205.

Figure 1 shows the calibrated *HST* data from both gratings. The typical S/N for measured fluxes is between 40 and 70 per resolution element (a diode in the detector) in both the G190H data (4000 s exposure) and the G270H data (1600 s exposure).

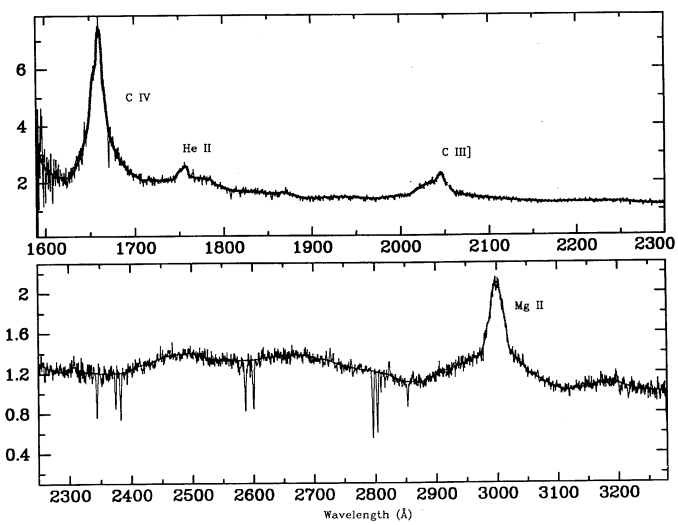


FIG. 1.—Ultraviolet spectrum of Mrk 205 taken with the *HST* Faint Object Spectrograph through the 0.″25 × 2.″0 slit. (*a*) Data obtained with the G190H grating from just below 1600 to 2300 Å. (*b*) Data from 2300 Å to the limiting red coverage of the G270H grating just longward of 3250 Å. Flux units are $10^{-14}$ ergs s$^{-1}$ cm$^{-2}$ Å$^{-1}$. Prominent emission lines are labeled. The smooth dark line is a "continuum" fit; see § 3.

## 3. THE CONTINUUM AND EMISSION LINES

Figure 1 shows that the overall properties of the ultraviolet spectrum of Mrk 205 are similar to that of other low-redshift AGNs: several broad emission lines appear on top of a relatively flat continuum. There are four prominent emission lines in the data: C IV λ1549, He II λ1640, C III] λ1909, and Mg II λ2800.

The first step in our analysis was to fit a smooth continuum to the data; the adopted shape is shown as a dotted line in Figure 1. The adopted continuum is our best estimate of the flux from the AGN before it encounters absorbing material in NGC 4319 or the Galaxy. Figure 1 shows that in addition to defining the continuum, the dotted line also attempts to recover the emission-line profile. This representation of the unabsorbed spectrum was used to determine the emission-line properties as well as providing the basis for selecting absorption lines (§ 4).

Comparing the continuum level shown in Figure 1 with the continuum determined by Kinney et al. (1991), we note that there is evidence for variability. The shapes of the continua determined by *IUE* and by *HST* are similar, but the *HST* continuum level appears to be higher by approximately 40%. The continuum level plotted by Kinney et al. (1991) is the median flux for the three *IUE* observations; Mrk 205 had a different mean flux level in each of the *IUE* observations (see Fig. 70 of Kinney et al. 1991).

We list in Table 1 the basic properties (center and observed equivalent widths) for the four prominent emission lines. These measurements were made by fitting a series of Gaussians to the line profile; the line centers are defined to be the center of the narrowest Gaussian component. The errors in the equivalent widths are dominated by the uncertainties in the continuum; the values listed in Table 1 were estimated from measurements of the lines using different representations of the continuum. The ratios of the strengths of the ultraviolet emission lines given here, especially C IV/C III] and C IV/Mg II, are more typical of quasars than of Seyfert I galaxies (see, e.g., Wu, Boggess, & Gull 1983), but are sensitively dependent upon how the broad wings or tails are treated in the measurements (see Fig. 1).

The emission line redshift of the AGN, $z_{em} = 0.0718 \pm 0.0020$, was calculated from the weighted average of three lines (the He II line was not used). The redshift found from the ultraviolet emission lines is in agreement with the redshift (0.070) found by Weedman (1970) and Bowen et al. (1991) using emission lines in the optical region of the spectrum.

## 4. MEASUREMENT OF ABSORPTION LINES

Figure 2 displays the 3 $\sigma$ limiting equivalent width for unresolved absorption lines as a function of wavelength, $EW_{limit}(\lambda)$, calculated for the observed *HST* spectrum of Mrk 205. The errors in the line strengths are calculated as in Young et al.

TABLE 1

SELECTED ULTRAVIOLET EMISSION-LINE PROPERTIES OF Mrk 205

| Line | $\lambda_{rest}$ (Å) | $\lambda_{obs}$ (Å) | $z_{em}$ | $EW_{obs}$ (Å) |
|---|---|---|---|---|
| C IV ..... | 1549.1 | 1659.6 ± 0.3 | 0.0714 | 57 ± 6 |
| He II ..... | 1640.5 | 1757.1 ± 2.0 | 0.0711 | 20 ± 15 |
| C III] ..... | 1909.0 | 2046.1 ± 0.3 | 0.0718 | 25 ± 8 |
| Mg II ..... | 2797.9 | 2999.5 ± 0.3 | 0.07205 | 55 ± 5 |

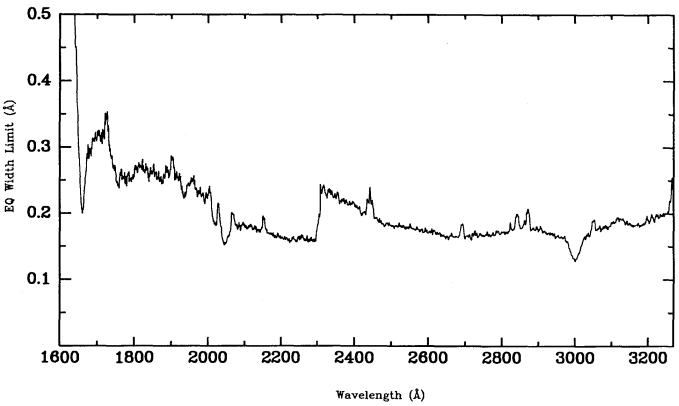


FIG. 2.—The 3 $\sigma$ equivalent width error (Å) for unresolved absorption lines is shown as a function of wavelength in the spectrum. To be included in the complete sample, a feature's equivalent width must exceed the value of the curve at the relevant wavelength.

(1979). The features of this curve can be understood by considering Figure 1: the broad dips are a reflection of the emission lines (higher signal in the lines results in a higher signal-to-noise ratio in the normalized spectrum), and the small "bumps" (most visible in the G270H data) are caused by diodes with low sensitivity. Strong absorption features, such as the interstellar lines, must be treated specially in order to avoid spurious "dips" in the limiting equivalent width table at the locations of the absorption lines. To produce an estimate of the sensitivity at the positions of the absorption lines, the flux errors of pixels whose fluxes fall more than 2 $\sigma$ below the continuum are replaced with the average error of the nearby continuum points. The effects of interstellar absorption lines are included explicitly in the identification procedures (see discussion of line-blocking in § 5, 8, and 9 of Bahcall et al. 1992).

Candidate absorption lines were marked independently by several of the authors on plots of the calibrated spectrum. The selection of absorption lines was checked with the aid of software that algorithmically recognizes absorption features (Schneider et al. 1992). All of the absorption features were fitted with single or, in the case of blends, multiple Gaussian profiles; line centers, dispersions, and equivalent widths were determined using IRAF. The weakest line that all authors agreed upon had equivalent widths of $\approx$0.20 Å; the strongest measured line that not all authors were convinced was real had an equivalent width of 0.25 Å. Several features whose strengths exceeded the limit were not included as they coincided with significant structure in the flat-field (see § 2).

Table 2 lists a complete sample of 12 absorption lines and one additional line, $\lambda$2260.5, that we believe is real but whose S/N (2.7) is not sufficient to be included in the complete sample. Here we define the S/N of a line as the ratio of the measured equivalent width of the line to the 1 $\sigma$ uncertainty in the measured value, S/N = $EW/\sigma(EW)$. The criterion for inclusion in the complete sample is a minimum observed equivalent width equal to 3 times the 1 $\sigma$ error at the line center:

$$EW_{\rm min}(\text{complete sample}; \lambda) = 3 \times \sigma(EW; \lambda) . \quad (1)$$

The individual columns in Table 2 contain the measured line center, observed equivalent width, signal-to-noise ratio of the line, identification, vacuum wavelength of identification, observed minus laboratory wavelength, $cz$ of extragalactic lines, and comments. The wavelength offsets for the two gratings were computed by requiring that the average velocity of the strong Galactic lines (see § 5) is zero.

In identifying the absorption lines, we allowed wavelength discrepancies as large as 1 Å or 3 times the estimated 1 $\sigma$ accuracy of the wavelength measurement, whichever is larger. All redshifts from zero to 30,000 km s$^{-1}$ larger than the emission line redshift were considered.

We first identified the interstellar lines from the Galaxy. These identifications are discussed in the following section (§ 5). There are only two lines listed in Table 2 that are not Galactic absorption lines; these two lines ($\lambda$2809 and $\lambda$2816) are discussed in § 6.

## 5. GALACTIC ABSORPTION LINES

Of the 12 observed lines in the complete sample, 10 are identified at zero redshift with strong lines from Galactic gas. Table 2 shows the 10 identifications of Galactic lines with Al II, Si II, Mg I, Mg II, Fe II, and Mn II. The average absolute value of the wavelength difference between the measured and the 10 rest wavelengths is 0.09 Å; the corresponding root-mean-squared difference is 0.11 Å. All lines that are expected to be present based upon abundance, atomic physics, and ionization considerations are identified in Table 2 (cf. Savage 1988). With only relatively minor differences, the same set of Galactic lines are observed in the direction of Mrk 205 ($l$ = 125°, $b$ = +42°),

TABLE 2

ULTRAVIOLET ABSORPTION LINES IN THE SPECTRUM OF Mrk 205: S/N = $EW(\lambda)/\sigma(EW; \lambda)$

| $\lambda_{\rm obs}$ (Å) | $EW$ (Å) | S/N | $z_{\rm abs}$[a] | Identification | | $\Delta\lambda$ (Å) | Comments |
|---|---|---|---|---|---|---|---|
| | | | | Ion | $\lambda_{\rm stnd}$ | | |
| 1670.72 | 0.41 | 7.1 | 0.000 | Al II | 1670.81 | −0.09 | |
| 1808.14 | 0.25 | 3.5 | 0.000 | Si II | 1808.00 | 0.14 | |
| 2344.18 | 0.83 | 11.8 | 0.000 | Fe II | 2344.21 | −0.03 | |
| 2374.51 | 0.62 | 8.7 | 0.000 | Fe II | 2374.46 | 0.05 | |
| 2382.75 | 0.84 | 12.8 | 0.000 | Fe II | 2382.76 | −0.01 | |
| 2586.87 | 1.03 | 16.4 | 0.000 | Fe II | 2586.64 | 0.23 | |
| 2600.26 | 1.04 | 16.5 | 0.000 | Fe II | 2600.18 | 0.08 | |
| 2796.25 | 1.43 | 30.6 | 0.000 | Mg II | 2796.35 | −0.10 | |
| 2803.46 | 1.21 | 23.9 | 0.000 | Mg II | 2803.53 | −0.07 | |
| 2809.14 | 0.25 | 4.6 | 0.00457 | Mg II | 2796.35 | 0.00 | Gas in NGC 4319 |
| 2816.02 | 0.17 | 3.0 | 0.00446 | Mg II | 2803.53 | 0.00 | Gas in NGC 4319 |
| 2853.07 | 0.46 | 6.9 | 0.000 | Mg I | 2852.97 | 0.10 | |

[a] Frame in which Galactic lines are at rest.

TABLE 3

COMPARISON OF GALACTIC ABSORPTION LINES IN THREE DIRECTIONS

| | | Equivalent Widths | | |
|---|---|---|---|---|
| Ion | λ (Å) | H1821+643 ($l = 94°$, $b = +27°$) | Mrk 205 ($l = 125°$, $b = +42°$) | 3C 273 ($l = 290°$, $b = +64°$) |
| Al II ..... | 1670.8 | 0.84 | 0.41 | 0.53 |
| Si II ..... | 1808.0 | Blend | 0.25 | <0.25 |
| Al III ..... | 1854.7 | <0.23 | <0.19 | 0.28 |
| Al III ..... | 1862.8 | <0.24 | <0.19 | 0·18 |
| Mg I ..... | 2026.5 | 0.21 | <0.17 | 0.27 |
| Fe II ..... | 2260.8 | 0.30 | <0.13 | <0.15 |
| Fe II ..... | 2344.2 | 1.10 | 0.83 | 0.73 |
| Fe II ..... | 2374.5 | 1.01 | 0.62 | 0.61 |
| Fe II ..... | 2382.8 | 1.38 | 0.84 | 0.83 |
| Mn II .... | 2576.9 | 0.44 | <0.17 | 0.34 |
| Fe II ..... | 2586.6 | 1.15 | 1.03 | 0.84 |
| Mn II .... | 2594.5 | 0.30 | <0.17 | 0.28 |
| Fe II ..... | 2600.2 | 1.47 | 1.04 | 0.98 |
| Mn II .... | 2606.5 | 0.20 | <0.17 | 0.16 |
| Mg II .... | 2796.4 | 1.86 | 1.43 | 1.10 |
| Mg II .... | 2803.5 | 1.77 | 1.21 | 0.99 |
| Mg I ..... | 2853.0 | 0.57 | 0.46 | 0.39 |

in the direction of 3C 273 ($l = 290°$, $b = +64°$), and in the direction of H1821+643 ($l$, $b$) = (94°, +27°).

In Table 3 we compare the Galactic lines observed with the FOS of *HST* in the directions of Mrk 205 (this paper), 3C 273 (Bahcall et al. 1991), and H1821+643 (Bahcall et al. 1992). As expected, the source with the lowest Galactic latitude, H1821+643, has the strongest Galactic absorption lines.

## 6. ABSORPTION BY GAS IN NGC 4319

Figure 3 shows the region near 2800 Å in the spectrum of Mrk 205. The two strongest absorption lines are of Galactic origin, Mg II λλ2803.53, 2796.35. The pair of absorption lines at λλ2809.14, 2816.02 is caused by gas in NGC 4319. The region marked FF in Figure 3 is affected by flat-field structure in the detector. We have examined this region of the spectrum in three calibration stars and have verified that the flat-field structure does not produce the features that we attribute to Mg II absorption by NGC 4319. We illustrate this result in Figure 4 which compares the spectrum of Mrk 205 in the region of interest with the spectra of three bright calibration stars. No feature of comparable strength to the Mg II doublet is seen in the five displayed calibration spectra.

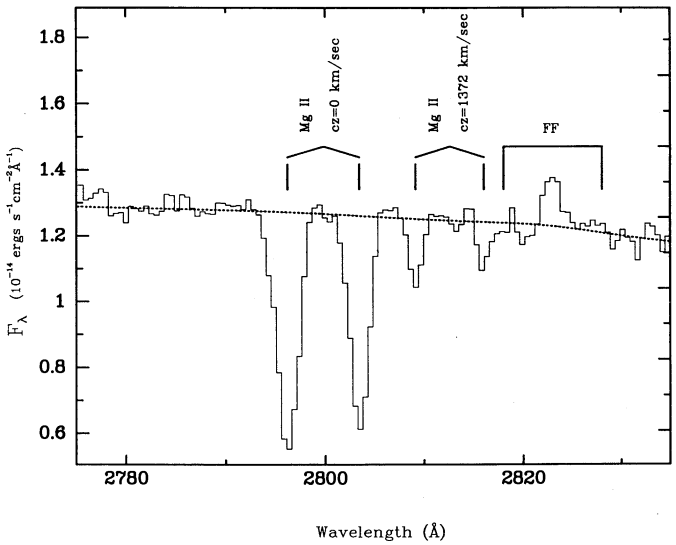


FIG. 3.—Spectrum of Mrk 205 near 2800 Å. The two strongest lines are of Galactic origin, Mg II λλ2803.53, 2796.5. The pair of absorption lines at λλ2809.15, 2816.02 is caused by gas in NGC 4319. The region marked FF is affected by flat-field structure in the detector.

Our best estimate for the heliocentric velocity of the Mg II absorption feature associated with NGC 4319 is

$$\langle cz \rangle_{\text{Mg II; heliocentric}} \approx 1265 \pm 55 \text{ km s}^{-1}. \qquad (2a)$$

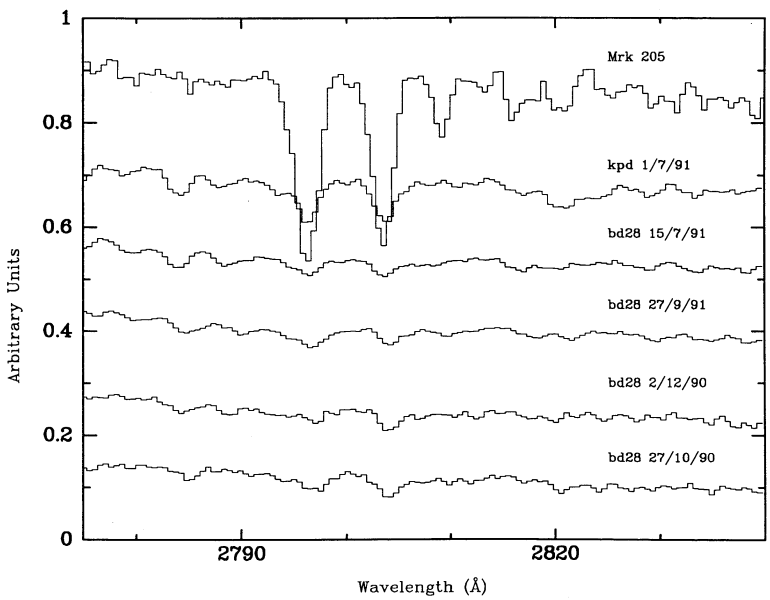


FIG. 4.—The figure compares, near 2800 Å, five spectra of calibration stars with the spectrum of Mrk 205. These data have been reduced to count rates but not corrected for flat-field defects. None of the spectra of the calibration stars shows a feature at 2809 or at 2816 Å of comparable strength to the features observed in the spectrum of Mrk 205.

The value given takes account of the average difference in velocity between the Galactic absorption lines and the local standard of rest and is based upon the measured velocity of the Mg II doublet from NGC 4319 relative to the strong Galactic lines, disk and halo (see § 4 and Table 2). The process we used to obtain the velocity presented in equation (2a) is described below.

The velocity of the NGC 4319 Mg II doublet relative to the Galactic lines is

$$\langle cz \rangle_{\text{Mg II; rel. to Galactic abs. lines}} = 1361 \pm 24 \text{ km s}^{-1}, \quad (2b)$$

where the indicated uncertainty includes the quadratically combined 1 $\sigma$ errors in the determination of the wavelength scale from measurements of the Galactic lines and in the wavelength measurements of the Mg II doublet. A direct measurement using an on-board calibration lamp spectrum obtained immediately following the Mrk 205 G270H observation indicates that we should subtract 96 $\pm$ 50 km s$^{-1}$ from the velocity measured with respect to the strong Galactic lines (eq. [2b]) in order to obtain the heliocentric velocity (eq. [2a]). The difference between the velocities given in equations (2a) and (2b) reflects the comparison with the calibration lamp. The reason for the relatively large difference between the two velocities is that the line of sight to Mrk 205 passes through a complex of high-velocity clouds (known as Complex C III to the aficionados; see Hulsbosch & Wakker 1988).

The heliocentric velocity of the nucleus of NGC 4319 was determined recently by Bowen et al. (1991) using seven lines in the blue spectrum of the galaxy and is

$$\langle V_H \rangle_{\text{nucleus}} = 1045 \pm 20 \text{ km s}^{-1}. \quad (2c)$$

On the other hand, the heliocentric velocity of NGC 4319 as measured by Sulentic & Arp (1987b) from the positions of Na I absorption and [N II] emission lines is

$$\langle V_H \rangle_{\text{Na I, [N II]}} = 1365 \text{ km s}^{-1}. \quad (2d)$$

The 140 km s$^{-1}$ spread in velocities in equations (2a)–(2d) is within the range of velocities observed for absorbing gas in the Galaxy.

Based upon the equivalent widths given in Table 2, the best-estimate column density and $b$-value of the Mg II gas in NGC 4319 are

$$N(\text{Mg II}) = 1.2 \times 10^{13} \text{ cm}^{-2}, \quad b = 12 \text{ km s}^{-1}. \quad (3)$$

The column density of Mg II gas could be as low as $5 \times 10^{12}$ cm$^{-2}$ if the true equivalent widths are lower, respectively, by 0.5 $\sigma$ and 1.0 $\sigma$ compared to the best-estimate values for the 2796 and 2803 Å lines. In this case, the doublet ratio would be equal to two, the optically thin limit. We are unable to set a useful upper limit on the column density since a doublet ratio equal to unity is allowed by the measurements without stretching beyond the 1 $\sigma$ limits. Formally, the total column density could be as much as $10^3$ larger than the best-estimate value given in equation (3), a result obtained by evaluating the expected line strengths for pure damping profiles.

Since NGC 4319 is nearly face-on, we cannot use geometrical or kinematical information to determine whether the absorbing gas is in the galaxy's disk or in the halo. Plausible scenarios could be constructed in which the absorption occurs in the disk, in the halo, or in both.

There are 17 strong resonance lines from low-ionization states of abundant ions that could be produced by interstellar or halo gas in NGC 4319, but which are not detected above our equivalent width limit (shown in Fig. 2). These unobserved lines are from Al II, Al III, Si II, Mg I, Fe II, and Mn II and are among the standard lines that are used in identifying quasar absorption lines (see Bahcall 1979; Morton 1991). Nearly all of the lines listed in Table 4 are observed to be strong Galactic absorption features (see Table 3 and Savage 1988).

Table 4 lists the 17 unobserved resonance lines and the upper limits to their equivalent widths.

## 7. SUMMARY AND CONCLUSIONS

We have detected absorption in the spectrum of the bright AGN Mrk 205 that is produced by Mg II ions in the intervening barred spiral galaxy NGC 4319. This result is consistent with the cosmological interpretation of the redshifts of both Mrk 205 and of NGC 4319, according to which the two objects are accidentally projected close to each other on the sky and the light from Mrk 205 passes through the disk and the halo of NGC 4319 on its way to the observer.

The stronger component of the Mg II doublet produced by gas in NGC 4319 (Fig. 3) has an equivalent width, 0.25 Å, that is about a factor of 5 smaller than the Mg II Galactic absorption lines observed in three different directions (Table 3; see also Savage 1988) and that is more than a factor of 10 weaker than the Mg II feature caused by the intervening galaxy NGC 3067 in the spectrum of the QSO 3C 232 (Kinney et al. 1991; Bowen et al. 1991). The equivalent widths of the Mg II lines produced by NGC 4319 gas are below the limiting sensitivity level of the complete samples of Mg II absorption in quasar spectra (mean absorption redshifts from 0.5 to 1.7) that are summarized in Table 1 of Bergeron (1988; see also Blades 1988).

We fail to detect absorption at the observed wavelengths that correspond to the rest wavelengths, for gas in NGC 4319, of 17 resonance lines from low-ionization states of abundant metals. The upper limits for possible absorption features from these lines are given in Table 4. These lines are generally detected as Galactic features in the spectra of extragalactic objects (see Table 3 and Savage 1988).

We expect that strong absorption from high-ionization ions such as C IV, Si IV, and N V will be detected when Mrk 205 is

TABLE 4

RESONANCE LINES NOT OBSERVED AT REDSHIFT OF NGC 4319

| $\lambda_{\text{obs}}$ (Å) | Ion | $\lambda_{\text{rest}}$ (Å) | $EW_{3\,\sigma\text{ upper limit}}$ (Å) |
|---|---|---|---|
| 1615.81 | Fe II | 1608.45 | 0.86 |
| 1678.46 | Al II | 1670.81 | 0.21 |
| 1816.27 | Si II | 1808.00 | 0.20 |
| 1863.21 | Al III | 1854.72 | 0.19 |
| 1871.30 | Al III | 1862.78 | 0.19 |
| 2035.74 | Mg I | 2026.47 | 0.15 |
| 2260.17 | Fe II | 2249.87 | 0.13 |
| 2271.11 | Fe II | 2260.76 | 0.13 |
| 2354.94 | Fe II | 2344.21 | 0.23 |
| 2385.33 | Fe II | 2374.46 | 0.21 |
| 2393.66 | Fe II | 2382.76 | 0.21 |
| 2588.68 | Mn II | 2576.89 | 0.17 |
| 2598.48 | Fe II | 2586.64 | 0.17 |
| 2606.37 | Mn II | 2594.50 | 0.17 |
| 2612.08 | Fe II | 2600.18 | 0.17 |
| 2618.40 | Mn II | 2606.47 | 0.17 |
| 2866.03 | Mg I | 2852.97 | 0.19 |

observed at shorter wavelengths with the *HST* spectrographs. The weakness of the absorption from low-ionization ions suggests that the illuminated gas in NGC 4319 is highly ionized. The value for the Mg II column density given in equation (3) can be used to estimate the column density of neutral hydrogen by assuming that the ratio of Mg II column density to H I column density is 1/10 the solar abundance ratio of magnesium to hydrogen. The resulting H I column density is about $3 \times 10^{18}$ cm$^{-2}$, which would produce a Ly$\alpha$ line with an equivalent width of 1.2 Å ($b < 30$ km s$^{-1}$).

We are grateful for valuable discussions with A. L. Kinney, A. Laor, D. Maoz, D. E. Osterbrock, J. P. Ostriker, and B. D. Savage. This work was supported in part by NASA contract NAG5-1618 and grant number GO-2424.01 from the Space Telescope Science Institute, which is operated by the Association of Universities for Research in Astronomy, Inc., under NASA contract NAS5-26555.

## REFERENCES

Arp, H. C. 1971, Astrophys. Lett., 9, 1
———. 1973, in The Redshift Controversy, by G. B. Field, H. Arp, & J. N. Bahcall (Reading, MA: W. A Benjamin), 15
Bahcall, J. N. 1973, in The Redshift Controversy, by G. B. Field, H. Arp, & J. N. Bahcall, 61
———. 1979, IAU Colloq. 54, Scientific Research with the Space Telescope, ed. M. S. Longair & J. W. Warner (Washington: GPO), 215
Bahcall, J. N., Jannuzi, B. T., Schneider, D. P., Hartig, G. F., Bohlin, R., & Junkkarinen, V. 1991, ApJ, 377, L5
Bahcall, J. N., Jannuzi, B. T., Schneider, D. P., Hartig, G. F., & Green, R. F. 1992, ApJ, 397, 68
Beaver, E. A., et al. 1991, ApJ, 377, L1
Bergeron, J. 1988, in QSO Absorption Lines, ed. J. C. Blades, D. Turnshek, & C. A. Norman (Cambridge: Cambridge Univ. Press), 127
Blades, J. C. 1988, in QSO Absorption Lines, ed. J. C. Blades, D. Turnshek, & C. A. Norman (Cambridge: Cambridge Univ. Press), 147
Blades, J. C., Wheatley, J. M., Panagia, N., Grewing, M., Pettini, M., & Wamsteker, W. 1988, ApJ, 344, 308
Bohlin, R. C., Harris, W. A., Holm, A. V., & Gry, C. 1990, ApJS, 74, 413
Bowen, D. V., Pettini, M., Penston, M. V., & Blades, C. 1991, MNRAS, 248, 153
Burbidge, G. R. 1988, Mercury, 17, 136
Ford, H. C. 1985, Faint Object Spectrograph Instrument Handbook (Baltimore: Space Telescope Science Institute)
Hulsbosch, A. N. N., & Wakker, B. P. 1988, A&AS, 75, 191
Kinney, A. L., Bohlin, R. C., Blades, J. C., & York, D. G. 1991, ApJS, 75, 645
Markarian, B. E. 1969, Astrofizika, 3, 55
Morton, D. C. 1991, ApJS, 77, 119
Savage, B. D. 1988, in QSO Absorption Lines, ed. J. C. Blades, D. Turnshek, & C. A. Norman (Cambridge: Cambridge Univ. Press), 195
Savage, B. D., & de Boer, K. S. 1981, ApJ, 243, 460
Schneider, D. P., et al. 1992, in preparation
Shuder, J. M. 1984, ApJ, 280, 491
Sulentic, J. W., & Arp, H. C. 1987a, ApJ, 319, 687
———. 1987b, ApJ, 319, 693
Véron-Cetty, M.-P., & Véron, P. 1991, A Catalogue of Quasars and Active Nuclei (5th ed.; Munich: European Southern Observatory)
Weedman, D. W. 1970, ApJ, 161, L113
Wu, C.-C., Boggess, A., & Gull, T. R. 1983, ApJ, 266, 28
Young, P. J., Sargent, W. L. W., Boksenberg, A., Carswell, R. F., & Whelan, J. A. J. 1979, ApJ, 229, 891